Southern Journal of Engineering & Technology – Special Issue, Vol. 01, Issue 01, 2024

Numerical Simulation of Soil Slope Stability Using Finite Element Method

Muhammad Hammad Shafqat[1], Naeem Mangi[1], Muhammad Saqib Hanif[1], Muhammad Rauf[1], Sulaiman Khan[2], Saifullah Mangi[3]

[1]School of Civil Engineering, Southwest Jiaotong University, Chengdu 610031, Sichuan, China

[2]Faculty of Geosciences and Environmental Engineering, Southwest, Jiaotong University, Chengdu 611756, China.

[3]Department of Civil Engineering, Quaid-e-Awan University of Science and Technology, Nawabshah, Pakistan

Abstract. The limit equilibrium *(LE)* techniques are normally applied for soil slope stability calculation in the field of geotechnical engineering. It is generally believed that the finite element based numerical techniques can provide more precise and sophisticated solutions as compared to LE approaches. Therefore, in this study, the stability of a soil slope is simulated via finite element-based method within the framework of ABAQUS software. The value of factor of safety *(FS)*, plastic strain and horizontal displacement are obtained to assess the stability of a given soil slope. Results showed that the FEM can obtain credible values of FS, plastic shear strain and horizontal displacement. The formation and possible location of plastic strain indicated that the location of critical failure surface is around the weak zone of slope. The possible failure of slope can be circular at the crest. The shear strength and slope geometry do not mobilize along the entire slip surface at the same time. Depending upon the angle of friction *(ϕ)* and cohesion force *(c)* of soil mass, the plastic zones may develop around the slip surface in which the circular shear failure of soil slope take place

Keywords: Finite Element Analysis; ABAQUS; Stability Analysis; Slip Surface; Soil Slope.

Email: m.hammad@my.swjtu.edu.cn,

1. Introduction

To develop proper transportation routes, slopes are excavating for desired connectivity and easy movement of vehicles. Excavation of slope and continuous weathering process disintegrates its shear strength result in slope failure. This causes significant fatalities, economic losses injuries, and property damages. In the past decades, a lot of methodologies have been proposed to mitigate the vulnerability caused by the slope failure (Hoek et al., 2000). Slope failure mechanisms mostly depends on material strength properties and slope geometry (Bhasin and Kaynia, 2004; Chuhan et al., 1997). Slope failure includes lateral spread, flow, slide landslides and sliding after loss of toe support (Highland and Bobrowsky, 2008).

The sliding surface delivers the necessary information about failure geometry and previously has been widely considered a helpful tool to accurately assess the stability constant of soil slope (Cheng and Lau, 2014). According to slope engineering, the slip surface is a surface that shows the smallest value of safety constant. The smallest value of FS has been calculated by studying circular arc with cohesion (c) over internal friction (ϕ) ratio (Hajiazizi and Tavana, 2013). The method of judgment the sliding surface is directly connected to the method of determining the minimum safety factor (Baker, 1980). To determine minimum FS for a sliding surface, limit equilibrium technique may allow a precise and an accurate evaluation method during large scale stability investigation.

However, LE approaches do not deliver the information about the location and distribution of slip surface. Therefore, it is more important to use a numerical model for proper estimation of failure surfaces of a soil slope.

Therefore, numerical tools provide much accurate results and these results are mostly used for delimiting the scope of landslide hazards and adjusting prevention and control plans. Existing studies often divide landslides into pre-instability stages. The current soil slope stability analysis methods mainly include the limit equilibrium method, hybrid methods, finite element methods and strength reduction techniques (Wang et al., 2024b). Finite element methods have been used for soil slope stability and failure analysis and the outcomes of these methods were very logical (Song et al., 2024a; Song et al., 2024b; Wang et al., 2024a). Material point method can evaluate very complex failure of slope (Basha and Raghuram, 2024; Li et al., 2024). Discontinuous deformation analysis is helpful under extreme rainfall and dynamic loading conditions (Li et al., 2024; Liu et al., 2024). Numerical manifold method has the ability to judge the deformation of heterogeneous slope material under water-bearing zone conditions (Cao et al., 2024; Xu et al., 2024; Yang et al., 2023). But finite element methods can be used to estimate the failure surface, FS and displacement of soil slope precisely (Chongzhi et al., 2024; Yang and Cheng, 2024).

In this study, a FE modeling program (ABAQUS) is used to investigate the stability of soil slope. Slope safety factor, failure surface and horizontal displacement are deeply analyzed using strength reduction method in ABAQUS software.

2. Study Area and Geology

The research site is Fort Munro hilly area. The Fort Munro hill station is situated near Dera Ghazi Khan City in Pakistan as shown in Fig. 1. The geology of slope is simply comprised of clay (cohesive soil) as show in Fig. 1. The site is located along the national highway N70. During extreme weathered condition slope slides on road. The coordinates (x and y) of slope were measured with total station as presented in Fig 1. The slope height is 14 m, length is 140 m and angle are 45°. Soil samples were collected during field investigation.

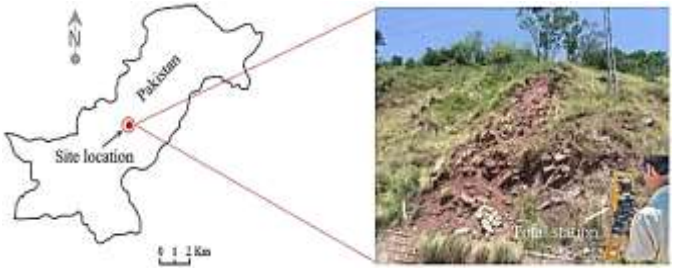

Fig. 1 Site location and topographical conditions of the selected slope

3. Methodology

In this research, direct shear test and uniaxial test were performed on soil samples to determine the shear strength properties. Then, the Fellenius slice method and a finite element method (FEM) were applied to determine the FS and the failure surfaces of soil slope. FEM method is based on a reduction process of shear strength properties of soil mass to calculate the FS of slope at failure stage. It is clear from the previous studies that the strength reduction technique in ABAQUS code could be effectively applied for the modeling of soil slope that shows circular failure (Chongzhi et al., 2024; Yang and Cheng, 2024). The reason is that soil is weak geological material which usually control the circular failure under normal conditions.

3.1. Experimental Results

Direct shear test and uniaxial test were performed on soil samples to estimate strength properties. Bulk density, cohesion force (c), Poisson's ratio and internal friction (ϕ) and Elastic modulus were determined using the laboratory results. The detail of these properties is presented in Table 1.

Table 1. Material parameters for the Slope

Bulk density (kN/m^3)	Cohesion (MPa)	Friction angle (°)	Poisson's Ratio	Elastic modulus (MPa)
21	0.04	22	0.28	102

3.2. Safety Factor Calculation

Fellenius slice method used here to estimate the safety factor of soil slope (Fellenius, 1936). This method adopts force components to estimate FS of a slope within the limit equilibrium state. In coordinate's direction, force components are always positive and act parallel to the failure surface. These could be described through a series of horizontal forces *(Pf)* and vertical forces *(Pr)* acting at the middle *(xi)* of each slice (Sengupta and Upadhyay, 2009). The factual points of each slice are usually defined with the moments *(My)* according to the horizontal *xi* forces (Baker, 1980). The analysis is carried out in terms of boundary water pressure and total unit weight. The external loads *(PI, Pr and M)* on the slope slip surface are considered as effect of water and *FS* is ratio between total resistance force *(ΣR)* and total sliding force *(ΣS)* as:

$$FS = \frac{\Sigma R}{\Sigma S} \quad (1)$$

In Eq. 1, FS is minimum safety factor, R is resistance force and *S* is sliding force. The initial tangential force *Ti* depends on effective cohesion (*ci*) and pore water pressure (*u*) and can be calculated via Eq. 2:

$$T_i = \frac{K_i}{F}[c_i + (N_i - u)\phi] \quad (2)$$

Were, ϕ is internal friction angle, *Ki* is cut-off function, *Ni* initial normal force of a slice and *F* is total horizontal force is sliding body. *Ki* can be defined as:

$$K_i = \{0\ if\ (Ni - u) < Si\ ,\quad K_i = \{1\ if\ (Ni - Ui) > Si \quad (3)$$

The total resistance force and total sliding force were calculated by using Eqs. 3-9:

$$0 \le Si \le \frac{Ci}{\psi i} \quad (4)$$

$$Pr = Fsp \cdot \Sigma T - [\Sigma\{(Ni - Ui) \cdot \tan\varphi\} + \Sigma(C \cdot l)] \quad (5)$$

$$N = W \cdot \cos\theta + QN \quad (6)$$

$$U = u \cdot b \cdot \cos\theta \quad (7)$$

$$T = W \cdot \sin\theta + QT \quad (8)$$

$$\Sigma(N - U)\tan\varphi + C \cdot \Sigma l = FS \cdot \Sigma T \quad (9)$$

Where, *Si* is tensile strength and *FS* is the factor of safety. *Pr* represents the prevention force, *Fsp* is assumed safety factor, *N* is normal force in slice and *b* is width of slice width. *T* shows the tangential force in slice, *l* is the slice length, *W* is slicing weight. θ is the dip angle of failure surface and *u* shows the water pressure. *QN* and *QT* are horizontal and vertical components of load, respectively. From above equations system, the upper limit consistent with linear Mohr-coulomb criterion and the lower limit corresponds to zero tensile strength.

4. Numerical Simulation

4.1. Model Parameters

A slope model was created in ABAQUS to compute *FS*, the location of slip surface and horizontal displacement. According to the slope dimensions and coordinates, a slope model was made in ABAQUS software by applying boundaries (Fig. 2). The bottom boundary was fixed and right and left boundaries were non-slip boundaries. The horizontal movement was constrained for all vertical boundaries. The grid size of 0.5m×0.5m was assigned in FE analysis. The size and shape of the finite elements were kept identical for soil strength parameters for accuracy. Soil strength properties assigned according to Table 1.

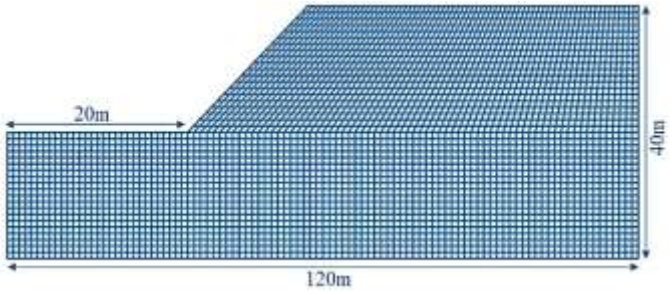

Fig. 2. Slope model in FEM analysis

4.2. Failure Criterion and FS

In finite element method, the Mohr-Coulomb failure criterion and elastoplastic constitutive model were selected for proper slope stability analysis. FEM has the ability to show the shear zones and slip surface of the slope with the help of plastic strain contour map (Melentijevic et al., 2017). The factor of safety was

evaluated in this subsection by using strength reduction approach *(SRM)* within the framework of FE modeling program. Strength reduction factor reduces the internal friction *(ϕ)* and cohesion *(c)* as follows:

$$c_r = \frac{c}{F} \quad (10)$$

$$\phi_r = tan - 1(\frac{tan\varphi}{F}) \quad (11)$$

Where: ϕr shows reduced internal friction and *cr* represents reduced cohesion force. F is reduction factor. Consequently, by using various trial values of F a series of simulations are accomplished until slope failure happens. The experimental value of reduction factor that causes the failure of soil slope is considered as the minimum safety constant (Xiao et al., 2016). For slope stability investigation, the failure condition is based on the relation of SRF values with displacements (Fig. 3). A relationship curve between horizontal displacement and the safety reduction factor (SRF) is plotted in Fig. 3. Inside the enormous number of interfaces, an abrupt change is detected in the horizontal displacement (Fig. 3). At abrupt change in displacement, the critical value of *SRF* is considered as the *FS* of the slope. Conferring to Fig. 3, the value of safety reduction factor *(SRF)* is 0.91 for the rock cut slope.

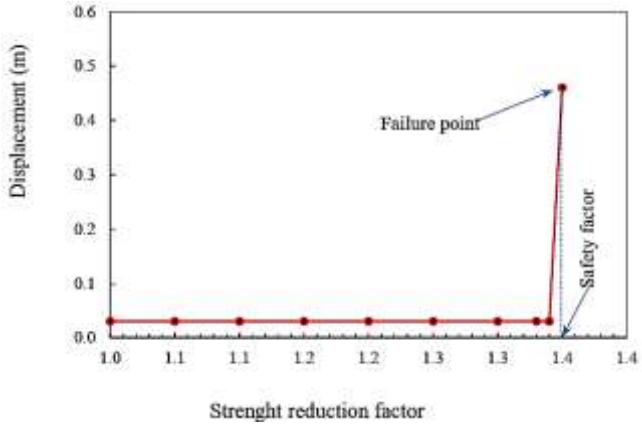

Fig. 3. Relationship between x-displacement SRF

4.3. Slope Stability Simulation

In this subsection, the stability of soil slope is simulated using the Mohr-Coulomb (M-C) principle. The contour maps of maximum principal stress and plastic strain of an unstable slope are plotted as can be shown in Figs. 4 and 5, respectively. As can be seen in Fig. 4 that the upper part of slope is subjected to tensile stress area at the certain depth from the crest. This is due to self-weight of slope. When the plastic strain band cut the slope as the instability criterion then the FS was 1.25 (Fig. 5). On the other hand, the corresponding plastic area of the slope attained via M-C principle could not show the tensile failure of slope crest. At this stage, the failure surface is a critical sliding body that propagate upward from the toe to the crest of the soil slope as can be seen in Fig. 5. The initial potential sliding surface of soil slope was located around area with high plastic strain.

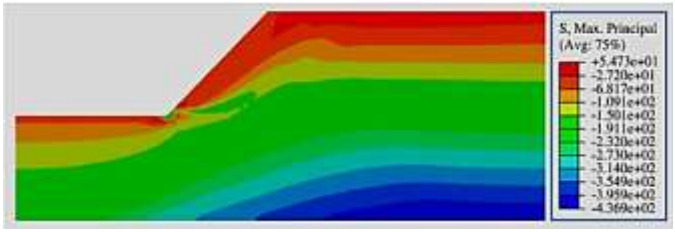

Fig. 4 Distribution of principal stress within slope

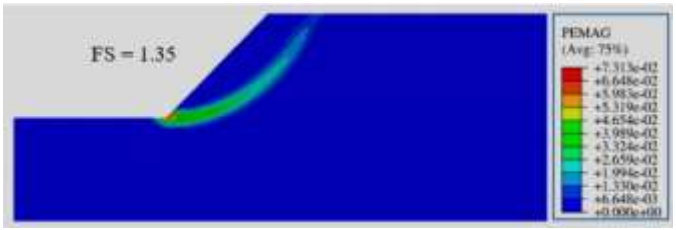

Fig. 5 Initiation of plastic strain from the toe of slope and FS

4.4. Development of Critical Slip Surface

Based on nonlinear yield principle, the development of critical slip surface (CSS) of soil slope is analyzed at different time intervals. Figure 6 displays the initiation of plastic zone (shear band) of an unstable soil slope. To evidently demonstrate the failure mechanism of a slip surface, three simulation phases are planned from the initial failure to the final failure of soil slope. The development of CSS depicted via contour map (color band) of correspondent plastic (shear) strain at various

time intervals (Fig. 6). The initial failure of slope started at T = 0.41s (Fig. 6a). The plastic strain zone formed at T = 0.44s as shown in Fig. 6(b). Next, it cut the entire slope at T = 0.53 (Fig. 6c) and finally, a slip surface is formed at T = 0.57 as shown in Fig. 6(d). The geometry of the CSS is observed to be circular. The reason is that weak zone is found in between the toe and top of slope and the CSS is always located near the plastic zone (weak zone). However, Fig. 6 displays the distribution weak areas and the upward propagation plastic strain from toe to crest.

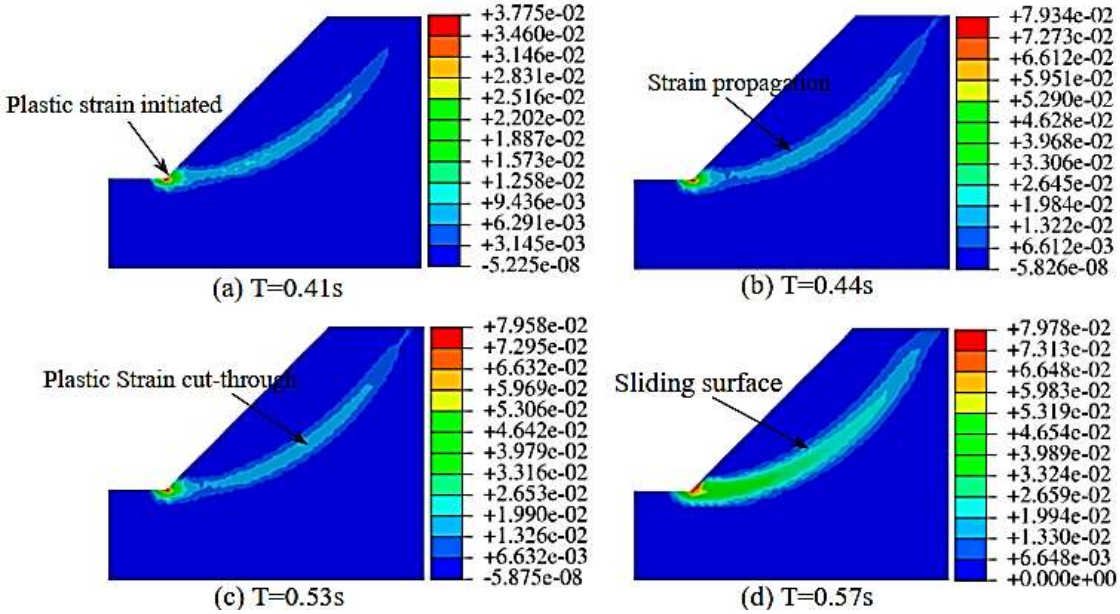

Fig. 6. Contour plot of plastic strain from FEM analysis

5. Parametric Study

In this section the x-displacement of slope at four different monitoring locations (A, B, C, D), influence of strength parameters (cohesion force and friction angle) and the influence of geometric parameters (slope angle and height) on FS are deeply studied for better understandings.

5.1. Horizontal Displacement

Fig. 7 shows the x-displacement of slope at four different monitoring locations (A, B, C, and D). It could be observed from Figure 7 that the x-displacement has different magnitude at each monitoring point. It increased with increasing the height of monitoring point (Fig. 7). At monitoring point, A (toe), the x-displacement of slope suddenly from 0 m to 0.5 when time rose from 0 to 7 s, respectively (Fig. 7). The maximum x-displacement of 0.8 m was noted near the crest of slope (Fig. 7). Overall, the horizontal displacement was noted around the crest of the slope. This is because of height that produces more gravity resulting in higher dis placement (Bowa and Xia, 2018).

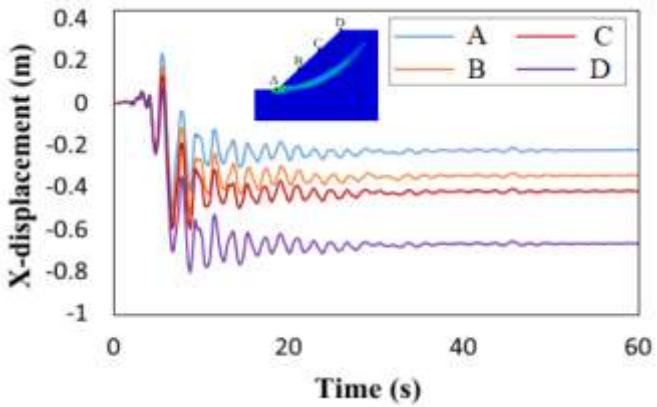

Fig. 7. Displacement history plot at four monitoring points

5.2. Effect of Strength Parameters on FS

With the purpose of investigating the effect of soil cohesion force on the minimum value of safety factor (FS) of slope three different values of cohesion (c), ranging from 0.01 MPa to 0.06 MPa were selected in in

two different methods (Fellenius and ABAQUS). The other soil constants, such as friction angle, unit weight and elasticity, were taken from Table 1. The changing effect of cohesion force on slope factor of safety is presented in Fig. 8(a). The cohesion parameter has a notable effect on slope safety constant (Fig. 8a). The safety factor of slope quickly rises as cohesion rise. The increasing trend of FS was same when Fellenius and ABAQUS methods were applied. But, ABAQUS produced a higher value of safety constant as compared to Fellenius method.

In order to analyze the impact of ϕ on slope safety constant, six different values friction angles ranging from 10o to 30o were chosen by adopting the method as for cohesion. The safety constant considerably effected by soil friction angle mainly for higher values (Fig. 8b). As the value of friction angle rise, the safety constant also rises. These numerical outcomes proved that friction angle and cohesion force of soil are resisting forces against failure.

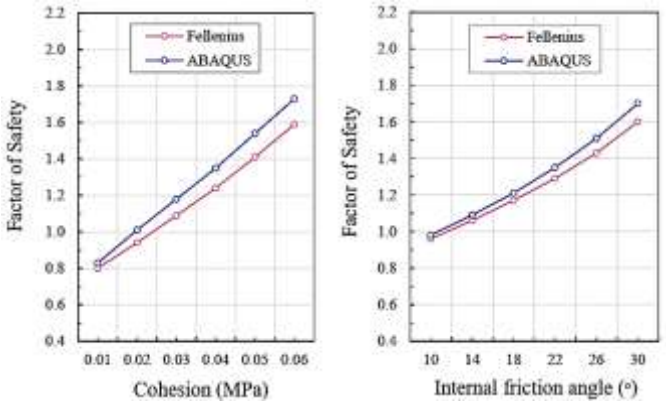

Fig. 8 (a) Influence of cohesion on FS and (b) influence of friction on FS

5.3. Effect of Slope Geometry on FS

In this subsection, the effect of slope geometry on safety constant is simulated by using FEM and Fellenius method. For this purpose, the value of slope angle (β) is ranging from 15o to 65o, and the value of slope height ranging from 15 m to 40 m. These values are according to site and engineering practice. The soil strength parameters were according to Table 1. The relationships between FS and β, and FS and H is plotted in Fig. 9. It is clear from the results that slope angle and height have a noticeable effect on slope safety constant (Fig. 9). As the value of β rise the slope safety constant also quickly rise (Fig. 9a). It is observed that by rising the value of slope angle, the slope become unstable, because higher value of β produces large failure surface, result in more shear force. Fig. 9(b) shows the relationship between slope safety constant and height (H). As slope height rise the safety constant slope decreased linearly. This could be got from Fig. 9(b) that the effect of H on slope safety constant is very notable. Slope FS quickly decreased as the value H increased as shown in Fig. 9(b). This is simply because of surcharge soil mass behaves as the overhead weight, which increases the sliding force result in decrease in FS.

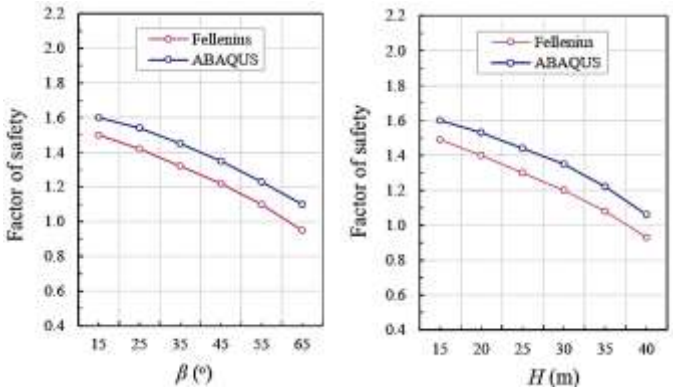

Fig. 9. Influence of slope profile on safety factor. (a) Influence of β and (b) influence of H

Based on numerical investigations, strain concentration and displacement history plot the possible failure of soil slope can be circular and failure surface can cut the slope form the toe.

6. Conclusions

In current study Fellenius slice method is used first to estimate the safety factor (FS) of soil beside NA70 in Pakistan. Then a Finite Element Method (FEM) within the framework of ABAQUS software were applied analyze the stability whole soil slope. The factor of safety of the slope is examined by strength reduction method. It is simulated via tensile stress and plastic strain

concentration x-displacement at given material properties. The maximum factor of safety of slope was 1.35, and the critical slip surface was located around the weak zone. Numerical outcomes revealed that a potential circular failure can take place at the upper portion of slope. The x-displacement rose with slope height and angle. The maximum x-displacement of 0.8 m was noted near the slope crest. Soil strength properties and geometric parameters have remarkable effect on slope FS. By decreasing these parameters result in decrease of slope FS. Based on numerical results and the contour plot of plastic strain, it can be well thought-out that the slope is unstable and need proper reinforcement.

Acknowledgement: Authors would like to Thanks Southwest University, Chengdu, China for financial support to conduct this research.

Data Availability Statement: Some or all data, models, or code that support the findings of this study are available from the corresponding author upon reasonable request.

Conflicts of Interest: The authors declare no conflict of interest.

References

Baker, R., 1980, Determination of the critical slip surface in slope stability computations: International Journal for Numerical and Analytical Methods in Geomechanics, v. 4, no. 4, p. 333-359.

Basha, B. M., and Raghuram, A. S. S. J. I. G. J., 2024, First-and second-order reliability analysis of rainfall-induced Kotropi slope failure, v. 54, no. 1, p. 266-283.

Bhasin, R., and Kaynia, A. M., 2004, Static and dynamic simulation of a 700-m high rock slope in western Norway: Engineering Geology, v. 71, no. 3-4, p. 213-226.

Bowa, V. M., and Xia, Y., 2018, Stability analyses of jointed rock slopes with counter-tilted failure surface subjected to block toppling failure mechanisms: Arabian Journal for Science and Engineering, v. 43, no. 10, p. 5315-5331.

Cao, X., Lin, S., Liang, Z., Guo, H., Zheng, H. J. C., and Geotechnics, 2024, Meshless numerical manifold method with novel subspace tracking and CSS locating techniques for slope stability analysis, v. 166, p. 106025.

Cheng, Y., and Lau, C., 2014, Slope stability analysis and stabilization: new methods and insight, CRC Press.

Chongzhi, W., Wang, Z. Z., Goh, S. H., Zhang, W. J. C., and Geotechnics, 2024, Comparing 2D and 3D slope stability in spatially variable soils using random finite-element method, v. 170, p. 106324.

Chuhan, Z., Pekau, O., Feng, J., and Guanglun, W., 1997, Application of distinct element method in dynamic analysis of high rock slopes and blocky structures: Soil Dynamics and Earthquake Engineering, v. 16, no. 6, p. 385-394.

Fellenius, W., Calculation of stability of earth dam, in Proceedings Transactions. 2nd Congress Large Dams, Washington, DC, 19361936, Volume 4, p. 445-462.

Hajiazizi, M., and Tavana, H., 2013, Determining three-dimensional non-spherical critical slip surface in earth slopes using an optimization method: Engineering geology, v. 153, p. 114-124.

Highland, L., and Bobrowsky, P. T., 2008, The landslide handbook: a guide to understanding landslides, US Geological Survey Reston.

Hoek, E., Read, J., Karzulovic, A., and Chen, Z. Y., Rock slopes in civil and mining engineering, in Proceedings ISRM International Symposium2000, International Society for Rock Mechanics.

Li, J., Wang, B., Pan, P., Chen, H., Wang, D., Chen, P. J. C., and Geotechnics, 2024, Failure analysis of soil-

rock mixture slopes using coupled MPM-DEM method, v. 169, p. 106226.

Liu, G., Meng, H., Song, G., Bo, W., Zhao, P., Ning, B., and Xu, X. J. E. E. S., 2024, Numerical simulation of wedge failure of rock slopes using three-dimensional discontinuous deformation analysis, v. 83, no. 10, p. 310.

Melentijevic, S., Serrano, A., Olalla, C., and Galindo, R., 2017, Incorporation of non-associative flow rules into rock slope stability analysis: International Journal of Rock Mechanics and Mining Sciences, v. 96, p. 47-57.

Sengupta, A., and Upadhyay, A., 2009, Locating the critical failure surface in a slope stability analysis by genetic algorithm: Applied Soft Computing, v. 9, no. 1, p. 387-392.

Song, X., Tan, Y., and Lu, Y. J. C., 2024a, Microscopic analyses of the reinforcement mechanism of plant roots in different morphologies on the stability of soil slopes under heavy rainfall, v. 241, p. 108018.

Song, X., Tan, Y. J. S., and Research, T., 2024b, Experimental study on the stability of vegetated earthen slopes under intense rainfall, v. 238, p. 106028.

Wang, H., Wang, Y., and Jin, F. J. W., 2024a, Stability of Expansive Soil Slopes under Wetting-Drying Cycles Based on the Discrete Element Method, v. 16, no. 6, p. 861.

Wang, H., Zou, J., Wang, X., Lv, P., Tan, Z., Cheng, L., Wei, Q., Qin, B., and Guo, Z. J. S. r., 2024b. Analysis of deformation mechanism of rainfall-induced landslide in the Three Gorges Reservoir Area: Piansongshu landslide, v. 14, no. 1, p. 10005.

Xiao, J., Gong, W., Martin II, J. R., Shen, M., and Luo, Z., 2016, Probabilistic seismic stability analysis of slope at a given site in a specified exposure time: Engineering geology, v. 212, p. 53-62.

Xu, B., Pei, X., Li, J., Yang, H., and Wang, X. J. C., 2024, Exploring the stability of unsaturated soil slope under rainfall infiltration conditions: A study based on multivariate interrelated random fields using R-vine copula, v. 234, p. 107587.

Yang, Y., Wu, W., Zheng, H. J. I. J. o. R. M., and Sciences, M., 2023, Investigation of slope stability based on strength-reduction-based numerical manifold method and generalized plastic strain, v. 164, p. 105358.

Yang, Z., and Cheng, X. J. T. G., 2024, High fill slope collapse: Stability evaluation based on finite element limit analyses, v. 44, p. 101156.